An empirical relation between velocity, mass discharge rate and vent area for normal through paroxysmal eruptions at Stromboli

Guillaume Georgeais, Andrew J. L. Harris, Yves Moussallam, Kenneth T. Koga, Estelle F. Rose-Koga

Type of Paper: Short Scientific Communication

An empirical relation between velocity, mass discharge rate and vent area for normal through paroxysmal eruptions at Stromboli

Guillaume Georgeais[1], Andrew J. L. Harris[2], Yves Moussallam[1,3], Kenneth T. Koga[4], Estelle F. Rose-Koga[4]

[1] *Lamont-Doherty Earth Observatory, Columbia University, New York, NY 10027, USA*

[2] *Université Clermont Auvergne, CNRS, IRD, OPGC, Laboratoire Magmas et Volcans, F-63000 Clermont-Ferrand, France*

[3] *Department of Earth and Planetary Sciences, American Museum of Natural History, New York, NY 10024, USA*

[4] *Institut des Sciences de la Terre d'Orléans (ISTO), UO/CNRS/BRGM, 1A rue de la Férollerie, 45071, Orléans, France*

✉ **Guillaume.Georgeais.pro@gmail.com**

Abstract

Based on published and new data for explosive events at Stromboli (Italy), we propose an empirical relation that links mass discharge rate (MDR) and at-vent gas jet velocity (G_v). We use 65 simultaneous measurements of MDR and G_v and find two trends in both the cross-correlation and rank order statistics. Cross-correlation gives a power law relation: $MDR = 10^{(0.015G_v+2.434)}$ kg/s, R^2=0.81, and applies to ash-dominated emissions. Combining this relation with the conservation of mass equation allows at-vent plume density and/or vent area to be derived from MDR = $G_v \rho A$, ρ being plume density and A being vent cross-sectional area. We find that while a vent radius of 2 m and plume density of 0.35 kg/m^3 fits with the "normal" activity at Stromboli, a 290 × 2.5 m vent area likely feeds a 10 kg/m^3 jet during paroxysmal activity. Initial tests on available data shows promise in extending the correlation beyond Stromboli and/or to events with higher MDR (>10^7 kg/s). However, the exact relation will depend on magma composition, temperature and volatile content, as well as conduit radius and vent overpressure.

Keywords: Thermal imagery, Eruption intensity, Mass Discharge Rate, Particle Velocity, Gas Jet Velocity, Stromboli

Acknowledgments

GG thanks Lucia Gurioli for her time and discussions about Stromboli volcano. We thank Larry Mastin and three other reviewers for their detailed and constructive comments and recommendations and Sara Barsotti for editorial handling.

Funding

GG was supported by a PhD fellowship from the French Government "Ministère de l'Enseignement Supérieur, de la Recherche et de l'Innovation". GG acknowledges the financial support from the laboratory of excellence ClerVolc for this project. This is contribution no. 601 of the ClerVolc program of the International Research Center for Disaster Sciences and Sustainable Development of the University of Clermont Auvergne.

Conflicts of interest/Competing interests

The authors declare no conflicts nor competing interest

Introduction

Mass Discharge Rate (MDR, kg/s) is commonly used to classify the "explosiveness" of a volcanic eruption, especially through the Volcanic Explosivity Index (Newhall and Self, 1982). Time-averaged MDR can be estimated from the total erupted mass divided by eruption duration (e.g., Mason et al. 2004; Bryan et al. 2010; Pyle, 2015). Peak MDR has also been derived from maximum plume height, as MDR is proportional to plume height to the power-of-four for Vulcanian-to-Plinian eruptions (Wilson et al. 1978). Geophysical signals, such as seismicity, infrasound and Doppler radar (e.g., Brodsky et al. 1999; Freret-Lorgeril et al. 2018; Perttu et al., 2020; Maki et al. 2021), as well as lightning intensity rates (Van Eaton et al., 2016), have also been tested as a proxy for MDR.

We propose a further option for deriving MDR from thermal or visible video using an empirical relation between MDR and gas jet velocity (G_v). We initially explore this relation for explosive events at Stromboli (Italy) where there is excellent constraint on the plumbing system (e.g., Bertagnini et al. 1999, 2013; Métrich et al. 2005, 2010, 2021), explosion source mechanisms (e.g., Chouet et al. 1999; Ripepe and Gordeev 1999; Ripepe et al. 2001) and emission dynamics (e.g., Patrick et al. 2007; Scharff et al. 2008; Gurioli et al. 2013). As a result data are available to test a relation between MDR and G_v. Stromboli also displays a range of explosive activity, which are commonly separated into three groups (Barberi et al. 1993). These are, in order of increasing magnitude: normal, major and paroxysmal. Named by Barberi et al. (1993) to describe the typical explosive activity that occurs at Stromboli, "normal" eruptions send 10–10^4 kg of bombs, gas and ash to a height of a few 10s to a few 100 m typically ~10 times an hour (Harris and Ripepe 2007; Patrick et al. 2007; Harris et al. 2013). Major eruptions can occur several times a year, involve 10^5–10^7 kg of bombs and ash, and send plumes to around a kilometre in height (Gurioli et al. 2013). Paroxysms are rarer, with four having occurred between 2003 and 2019, and form buoyant ash-rich plumes that ascend to several kilometres, and involve >10^8 kg (Rosi et al., 2006; Pistolesi et al. 2011; Giordano and De Astis 2020).

The wealth of data for explosions at Stromboli makes it an ideal location to test relations between a variety of eruption source terms (e.g., MDR and vent area) and plume ascent parameters (e.g., emission velocity and plume ascent velocity). We thus use Stromboli to explore an empirical relation between at-vent gas velocity and MDR using published and new datasets for which the two parameters can be simultaneously derived.

Method

We examined 65 eruptive events (59 normal, two major and four paroxysmal) for which suitable data were available (Table 1). Harris et al. (2013) obtained the mass (m) of 21 normal eruptions from thermal video using the amount of energy lost by the bomb field during cooling.

However, the duration (*t*) for these events was not assessed, so we revisited the data to obtain emission duration so that time-averaged MDR could be obtained from *m/t*. Duration was taken as the time between the first appearance of the plume and the last bomb to exit the vent. Videos used were recorded at 30 frames per second, and in the compressed data 10 frames were equivalent to one second of recording. The uncertainty is five frames (0.5 s), so that (considering the same uncertainty for the start and end of the event) error on duration is ±1 s.

We also used the mass, particle ejection velocity and duration 31 eruptions as obtained by Bombrun et al. (2015) through particle tracking to convert to time-averaged MDR. In addition, we included MDR and gas ejection velocities for transient ash-dominated normal eruptions at Stromboli as derived from thermal and visible imagery by Tournigand et al. (2017).

Mass discharge rates for major and paroxysmal eruptions at Stromboli were taken from the literature as follows:

- For the 8 and 24 November 2009 major eruptions MDR was taken from Gurioli et al. (2013);
- For the 2003 and 2007 paroxysms, we used the MDR of Rosi et al. (2006) and Pistolesi et al. (2011), respectively;
- MDR for the July and August 2019 paroxysms were calculated from maximum plume height by Giordano and De Astis (2020) following the equation of Mastin et al. (2009).

A theoretical relation between ballistic exit velocity (*Bv*) and gas exit velocity (*Gv*) was proposed by Steinberg and Babenko (1978). In this relation, *Gv* represents the speed of the gas to which the finest particles are coupled, and *Bv* represents the velocity of particles large enough to be affected by drag, as tested on and applied to normal eruptions at Stromboli by Ripepe et al. (1993) and Harris et al. (2012b).

Ballistic velocities are obtained either through particle tracking and given by Harris et al. (2013) and Bombrun et al. (2015) for normal explosions, or ballistic trajectory modeling for major (Gurioli, Colo, et al., 2013; Pioli et al., 2014) and paroxysmal events (Rosi et al., 2006; Pistolesi et al., 2011; Andronico et al., 2013; Giordano & De Astis, 2020). We convert these ballistic velocities (B_v) to gas jet velocities (G_v^b) using equation (8) of Harris et al. (2012b):

$$G_v^b = 1.41 \times B_v + 15.3 \quad (1)$$

This relation is set for explosions at Stromboli and correlates well with directly measured gas ejection velocities (Fig. 1). The literature-derived database is given in Table 1, and our calculated MDR data are given in Table 2.

Results

The 21 normal explosions at Stromboli recorded by Harris et al. (2013) lasted between 3 and 28 seconds, giving MDRs ranging from 32 to 800 kg/s (Table 2). Eruptions from vent NE1 lasted longer (average of 18 s) than eruptions from NE2 (average of 6 s). This leads to a wider range of MDR values for events at NE2 than NE1 (Fig. 2a). In Figure 2a, data from Bombrun et al. (2015) fall in a cluster of low MDR and high gas velocities (150–250 m/s, MDR < 10^4 kg/s), and data from Tournigand et al. (2017) have high MDR with low gas velocities (<150 m/s, MDR ≥ 10^4 kg/s). MDR for these normal explosions show correlations with gas velocity with an R^2 of between 0.5 and 0.83 depending on the data set used (Fig. 2a).

MDR for the major and paroxysmal events range between 10^4 and 10^7 kg/s, with gas jet velocities in the range 142–297 m/s (Table 1). The relation between MDR and gas velocity for the six major and paroxysmal explosions shows a positive, linear correlation with an R^2 of 0.79.

Eruption magnitudes have a power-law dependence (Pyle, 1998). This can be expressed as a rank order plot, as obtained by sorting the values from the highest to the lowest (Sornette et al. 1996). This method can be used to constrain whether the dataset is homogeneous (cf. Schneider

and Barbera, 1998) within a single volcanic system. The rank order plot for our Stromboli data shows two trends representing two different populations (Fig. 3). These two populations are apparent in the rank order statistics for both gas velocity and MDR and involve a first group of low gas velocity and MDR, and a second group of high gas velocity and MDR. We thus define two main populations and treat them separately. The first involves ballistic-dominated normal emissions (Fig. 2a). The second includes all major and paroxysmal events, plus one ash-dominated normal eruption, this population being of ash-rich emissions involving plume ascent dominated by buoyancy (Fig. 2b)

Discussion

The two trends apparent for Stromboli in the cross-correlation (Fig. 2) and rank order (Fig. 3) plots result from the different plume types considered and differences in their associated ascent dynamics. Normal explosions at Stromboli are associated with slug flow in the conduit (Gonnermann and Manga, 2012) and are characterized by very low levels of fragmentation to produce bomb-dominated plumes with particles that follow ballistic trajectories (e.g., Chouet et al. 1974; Patrick et al. 2007; Gurioli et al. 2013). In contrast, major and paroxysmal events involve rapid ascent of magma coupled with a gas phase ascending from depths of 7–10 km and are characterized by higher degrees of fragmentation (e.g., Bertagnini et al. 1999; Métrich et al. 2005, 2010, 2021; Pioli et al. 2014). The result is an ash-dominated plume whose ascent is characterized by a longer steady convection-dominated phase (cf. Wilson and Self 1980; Rosi et al. 2006; Harris et al. 2008).

Cross-correlation using data for ballistic-dominated normal explosions at Stromboli gives a relation between MDR and G_v of (Fig. 2a, yellow regression line):

$$MDR = 10^{(0.003G_v + 1.933)} \qquad R^2 = 0.50 \quad (2a)$$

Considering only a single vent improves the correlation, where the relation for vent NE1 (Fig. 2a, blue regression line) is:

$$MDR = 10^{(0.004G_v+1.906)} \quad R^2 = 0.83 \quad (2b)$$

These two relations are consistent with differences in vent size, gas/particle ratio, crater geometry, overpressure and volatile content between craters and events.

Finally, the cross-correlation for ash-dominated normal, major and paroxysmal events gives

$$MDR = 10^{(0.015G_v+2.434)} \quad R^2 = 0.81 \quad (3)$$

This is the black regression line of Figure 2b.

The next largest event at Stromboli?

Application of maximum likelihood statistics to our rank order plots (cf. Sornette et al. 1996; Pyle 1998) can indicate the most probable MDR and gas velocity for the hypothetical, but next largest, eruption not recorded in our data (i.e., an event larger than the 2003 paroxysm). On this basis an eruption at Stromboli larger than the 2003 paroxysm would have an MDR of 2.19 × 10^7 kg/s and a gas ejection velocity of 338 m/s. Our current data set for Stromboli is missing at least two paroxysms, i.e., those of 1456 and 1930. Both have been described as being larger than the 2003 paroxysm (e.g., Rosi et al. 2006; Bertagnini et al. 2011; Métrich et al. 2021), but both lack an assessment of MDR and G_v. We thus speculate that the MDR and G_v calculated for the next largest eruption in our dataset are possibly representative of the 1456 and 1930 paroxysms.

Vent size during normal and paroxysmal activity

MDR is related to bulk average (V) velocity, gas-particle mixture density (ρ) and vent cross sectional area, A:

$$MDR \approx \rho VA \quad (4)$$

Given a vent radius typical for Stromboli, i.e., 2 m (Harris et al. 2012b), we use our range of ejection velocities and MDR values to solve for mixture density. We find that the normal gas and ballistic-dominated events fit with a cloud density of 0.35 kg/m^3 (Fig. 2a). This corresponds

to the density of water vapor at 650 K. Instead, ash-dominated normal events fit with 10 kg/m^3 (Fig. 2a). Note, that these values are for at-vent conditions and are hence in the gas-thrust region of the jet before entrainment of air.

The lower and higher limits of the data set for major and paroxysmal eruptions can only be reproduced with a cloud density of 10 and 2600 kg/m^3, respectively (Fig. 2b). The latter density is close to the dense-rock value of basaltic magma, and does not provide a realistic plume density. For paroxysmal eruptions the conduit radius likely exceeds 2 m. Using the MDR and G_v for the July 2019 paroxysm (Table 1), with a cloud density of 10 kg/m^3, gives a circular vent radius of ~13 m. A 290 m long and 2.5 m wide source also provides a fit for the paroxysmal events. This would represent an eruption from the entire length of a SW-NE trending dyke underlying the crater terrace, and is consistent with emission from all three active craters during a paroxysm (Rosi et al., 2006). It is also consistent with collapse of the crater terrace following paroxysms to create a continuous trench in place of the typical three-crater system that characterizes Stromboli's crater terrace during normal activity (cf. Harris and Ripepe, 2007) and the ejection of meter-sized blocks of the "shattered shallow subvolcanic system" (Renzulli et al., 2009).

We calculate the at-vent volume fraction of pyroclasts (f) within the plume using a simple mixture model:

$$\rho \approx f \times \rho_{pyroclast} + (1 - f) \times \rho_{gas} \quad (5)$$

An average pyroclast density ($\rho_{pyroclast}$) of ~800 kg/m^3 (Pichavant et al. 2022), a gas density (ρ_{gas}) of 0.35 kg/m^3 (Harris et al. 2013), and a plume density of 10 kg/m^3 results in a mixture of ~1 % pyroclasts and ~99 % gas volumes (respectively ~97 % pyroclasts and ~3 % gas mass fraction) . A low gas weight fraction indicates that the cloud was ejected out of the vent without any mixing with the atmosphere (Wilson and Self, 1980).

Towards a global predictive model for eruption intensity?

At-vent gas and particle velocities vary as a function of vent geometry, over-pressure, magma temperature, volatile content, particle size and gas density (Steinberg and Babenko, 1978; Woods and Bower, 1995). By restricting our consideration to a single system, we limit the variation in volatile content, temperature, crater/vent geometry, pressure, ash/gas ratio, and gas density. Our results for Stromboli indicate that, if eruption types and styles are considered separately according to their dynamics, and measurements of mass eruption rate, gas velocity and particle velocity are available, then an empirical relation relating the three can be derived. We assess whether this can be extended to other, higher magnitude systems by considering:

- Pinatubo 1991 (VEI = 6; based on the data from Simkin et al, 1981);
- Mt. St. Helens 1980 (VEI = 5; Venzke 2022);
- Fuego 2012 (VEI ≤ 2; Venzke 2022);
- Sakurajima 2013 (VEI ≤ 3; Venzke 2022).

For Fuego and Sakurajima we take the MDR and G_v as derived from thermal and visible imagery by Tournigand et al. (2017). For Pinatubo, an MDR ranging between 6.8×10^8 and 10^9 kg/s has been calculated from granulometry (Koyaguchi and Ohno 2001) and satellite data (Koyaguchi and Tokuno 1993). MDR estimates for Mt. St. Helens range from an average of 2×10^7 kg/s for the whole eruption (Carey and Sigurdsson, 1985; Pyle, 2015), to $2–6 \times 10^9$ kg/s for the initial lateral blast (Brodsky et al. 1999). In all cases, we use the full range. For Pinatubo whether we calculate gas velocity using the at-vent decompressing jet model (6) or the freely decompressing model (7) of Woods and Bower (1995) is debatable:

$$G_v = 0.95 \times (n_0 RT)^{1/2} \quad (6)$$

$$G_v = 1.85 \times (n_0 RT)^{1/2} \quad (7)$$

Here n_0 is the difference between melt inclusion volatile concentration (6.4–7 wt %, Rutherford and Devine, 1996) and glass matrix average volatile concentration (1.45 wt.%, Hammer et al., 1999), R is the vapor-gas constant (461.5 J/kg K), and T is the magma temperature (1073 K). The value we obtain is likely a maximum since experimental studies suggested disequilibrium degassing for this eruption (Mangan and Sisson, 2000), which would delay nucleation and thus decrease magma ascent rate and G_v. For Mt. St. Helens we use the range of velocities for the Plinian phase given by Carey and Sigurdsson (1985) and Woods and Bower (1995), i.e., 200–300 m/s. We use velocities as close as possible to the vent-leaving values, where the at-surface decompression of the volcanic jet has the least impact (Woods and Bower, 1995) and where vent-leaving values can be compared between cases.

MDR values for Sakurajima, Pinatubo, and Mt. St. Helens are one-to-three orders of magnitude higher than those for Stromboli and Fuego at similar G_v (Fig. 4). However, the relationship between G_v and MDR remains linear and positive. This is consistent with the decompressing jet model of Woods and Bower (1995) for the emission dynamics of gas-particle mixtures, where variations in magma volatile content, over-pressure, vent geometry, and magma temperature account for the differences observed between each system (Fig. 4).

Conclusion

We derive an empirical relationship between gas jet velocity and MDR which applies to explosive events at Stromboli with VEI ranging from 0 to 3. At Stromboli, a network of continuously recording thermal cameras allows measurement of gas jet velocity (Delle Donne and Ripepe, 2012). This means that real-time measurements of G_v can potentially be converted to MDR for the two event types (ballistic and convective emissions) common at this well-monitored site.

Extending the analysis to events with higher VEI suggest a wider applicability a linear relation between G_v and MDR. Our argument is thus for a database with simultaneous measurements

of MDR and at-vent velocities for a variety of systems, allowing extension of this analysis. Such data requires a video camera network targeting the vent, which is rarely possible. All the same, given the importance of MDR as a key source term in forward modeling (cf. Bonadonna et al. 2011), such a fast and straightforward empirical approach to potentially derive MDR in near-real time shows promise.

References

Andronico, D., Taddeucci, J., Cristaldi, A., Miraglia, L., Scarlato, P., & Gaeta, M. (2013). The 15 March 2007 paroxysm of Stromboli: video-image analysis, and textural and compositional features of the erupted deposit. *Bulletin of Volcanology*, *75*(7), 733. https://doi.org/10.1007/s00445-013-0733-2

Bertagnini, A., Coltelli, M., Landi, P., Pompilio, M., & Rosi, M. (1999). Violent explosions yield new insights into dynamics of Stromboli volcano. *Eos, Transactions American Geophysical Union*, *80*(52), 633–636. https://doi.org/10.1029/99EO00415

Bertagnini, Antonella, Di Roberto, A., & Pompilio, M. (2011). Paroxysmal activity at Stromboli: lessons from the past. *Bulletin of Volcanology*, *73*(9), 1229–1243. https://doi.org/10.1007/s00445-011-0470-3

Bertagnini, Antonella, Méltrich, N., Francalanci, L., Landi, P., Tommasini, S., & Conticelli, S. (2013). Volcanology and Magma Geochemistry of the Present-Day Activity: Constraints on the Feeding System. In S. Calvari, S. Inguaggiato, G. Puglisi, M. Ripepe, & M. Rosi (Eds.), *Geophysical Monograph Series* (pp. 19–37). Washington, D. C.: American Geophysical Union. https://doi.org/10.1029/182GM04

Bevilacqua, A., Bertagnini, A., Pompilio, M., Landi, P., Del Carlo, P., Di Roberto, A., et al. (2020). Major explosions and paroxysms at Stromboli (Italy): a new historical catalog and temporal models of occurrence with uncertainty quantification. *Scientific Reports*, *10*(1), 17357. https://doi.org/10.1038/s41598-020-74301-8

Bombrun, M., Harris, A., Gurioli, L., Battaglia, J., & Barra, V. (2015). Anatomy of a Strombolian eruption: Inferences from particle data recorded with thermal video. *Journal of Geophysical Research: Solid Earth*, *120*(4), 2367–2387. https://doi.org/10.1002/2014JB011556

Bonadonna, C., Genco, R., Gouhier, M., Pistolesi, M., Cioni, R., Alfano, F., et al. (2011). Tephra sedimentation during the 2010 Eyjafjallajökull eruption (Iceland) from deposit, radar, and satellite observations. *Journal of Geophysical Research: Solid Earth*, *116*(B12). https://doi.org/10.1029/2011JB008462

Brodsky, E. E., Kanamori, H., & Sturtevant, B. (1999). A seismically constrained mass discharge rate for the initiation of the May 18, 1980 Mount St. Helens eruption. *Journal of Geophysical Research: Solid Earth*, *104*(B12), 29387–29400. https://doi.org/10.1029/1999JB900308

Bryan, S. E., Peate, I. U., Peate, D. W., Self, S., Jerram, D. A., Mawby, M. R., et al. (2010). The largest volcanic eruptions on Earth. *Earth-Science Reviews*, *102*(3–4), 207–229. https://doi.org/10.1016/j.earscirev.2010.07.001

Carey, S., & Sigurdsson, H. (1985). The May 18, 1980 eruption of Mount St. Helens: 2. Modeling of dynamics of the Plinian Phase. *Journal of Geophysical Research: Solid Earth*, *90*(B4), 2948–2958. https://doi.org/10.1029/JB090iB04p02948

Chouet, B., Hamisevicz, N., & McGetchin, T. R. (1974). Photoballistics of volcanic jet activity at Stromboli, Italy. *Journal of Geophysical Research (1896-1977)*, *79*(32), 4961–4976. https://doi.org/10.1029/JB079i032p04961

Chouet, B., Saccorotti, G., Dawson, P., Martini, M., Scarpa, R., De Luca, G., et al. (1999). Broadband measurements of the sources of explosions at Stromboli Volcano, Italy. *Geophysical Research Letters*, *26*(13), 1937–1940. https://doi.org/10.1029/1999GL900400

Delle Donne, D., & Ripepe, M. (2012). High-frame rate thermal imagery of Strombolian explosions: Implications for explosive and infrasonic source dynamics. *Journal of Geophysical Research: Solid Earth*, *117*(B9). https://doi.org/10.1029/2011JB008987

Freret-Lorgeril, V., Donnadieu, F., Scollo, S., Provost, A., Fréville, P., Guéhenneux, Y., et al. (2018). Mass Eruption Rates of Tephra Plumes During the 2011–2015 Lava Fountain Paroxysms at Mt. Etna From Doppler Radar Retrievals. *Frontiers in Earth Science*, *6*, 73. https://doi.org/10.3389/feart.2018.00073

Giordano, G., & De Astis, G. (2020). The summer 2019 basaltic Vulcanian eruptions (paroxysms) of Stromboli. *Bulletin of Volcanology*, *83*(1), 1. https://doi.org/10.1007/s00445-020-01423-2

Global Volcanism Program, & Venzke, E. (2022). Volcanoes of the World, v.5 [Data set]. Global Volcanism Program.

Gonnermann, H., & Manga, M. (2012). Dynamics of magma ascent in the volcanic conduit Chapter 4 Overview. https://doi.org/10.1017/cbo9781139021562.004

Gurioli, L., Harris, A. J. L., Colò, L., Bernard, J., Favalli, M., Ripepe, M., & Andronico, D. (2013). Classification, landing distribution, and associated flight parameters for a bomb field emplaced during a single major explosion at Stromboli, Italy. *Geology*, *41*(5), 559–562. https://doi.org/10.1130/G33967.1

Gurioli, L., Colo, L., Bollasina, A. J., Harris, A. J. L., Whittington, A., & Ripepe, M. (2013). Dynamics of Strombolian explosions: Inferences from field and laboratory studies of erupted bombs from Stromboli volcano. *Journal of Geophysical Research*, 27.

Hammer, J. E., Cashman, K. V., Hoblitt, R. P., & Newman, S. (1999). Degassing and microlite crystallization during pre-climactic events of the 1991 eruption of Mt. Pinatubo, Philippines. *Bulletin of Volcanology*, *60*(5), 355–380. https://doi.org/10.1007/s004450050238

Harris, A., & Ripepe, M. (2007). Synergy of multiple geophysical approaches to unravel explosive eruption conduit and source dynamics – A case study from Stromboli. *Geochemistry*, *67*(1), 1–35. https://doi.org/10.1016/j.chemer.2007.01.003

Harris, A.J.L., Delle Donne, D., Dehn, J., Ripepe, M., & Worden, A. K. (2013). Volcanic plume and bomb field masses from thermal infrared camera imagery. *Earth and Planetary Science Letters*, *365*, 77–85. https://doi.org/10.1016/j.epsl.2013.01.004

Harris, Andrew J. L., Ripepe, M., Calvari, S., Lodato, L., & Spampinato, L. (2013). The 5 April 2003 Explosion of Stromboli: Timing of Eruption Dynamics Using Thermal Data. In S. Calvari, S. Inguaggiato, G. Puglisi, M. Ripepe, & M. Rosi (Eds.), *Geophysical Monograph Series* (pp. 305–316). Washington, D. C.: American Geophysical Union. https://doi.org/10.1029/182GM25

Harris, Andrew J.L., Ripepe, M., & Hughes, E. A. (2012). Detailed analysis of particle launch velocities, size distributions and gas densities during normal explosions at Stromboli. *Journal of Volcanology and Geothermal Research*, *231–232*, 109–131. https://doi.org/10.1016/j.jvolgeores.2012.02.012

Koyaguchi, T., & Ohno, M. (2001). Reconstruction of eruption column dynamics on the basis of grain size of tephra fall deposits: 2. Application to the Pinatubo 1991 eruption. *Journal of*

Geophysical Research: Solid Earth, *106*(B4), 6513–6533. https://doi.org/10.1029/2000JB900427

Koyaguchi, T., & Tokuno, M. (1993). Origin of the giant eruption cloud of Pinatubo, June 15, 1991. *Journal of Volcanology and Geothermal Research*, *55*(1), 85–96. https://doi.org/10.1016/0377-0273(93)90091-5

Leduc, L., Gurioli, L., Harris, A., Colò, L., & Rose-Koga, E. F. (2015a). Types and mechanisms of strombolian explosions: characterization of a gas-dominated explosion at Stromboli. *Bulletin of Volcanology*, *77*(1), 8. https://doi.org/10.1007/s00445-014-0888-5

Leduc, L., Gurioli, L., Harris, A., Colò, L., & Rose-Koga, E. F. (2015b). Types and mechanisms of strombolian explosions: characterization of a gas-dominated explosion at Stromboli. *Bulletin of Volcanology*, *77*(1), 8. https://doi.org/10.1007/s00445-014-0888-5

Maki, M., Kim, Y., Kobori, T., Hirano, K., Lee, D.-I., & Iguchi, M. (2021). Analyses of three-dimensional weather radar data from volcanic eruption clouds. *Journal of Volcanology and Geothermal Research*, *412*, 107178. https://doi.org/10.1016/j.jvolgeores.2021.107178

Mangan, M., & Sisson, T. (2000). Delayed, disequilibrium degassing in rhyolite magma: decompression experiments and implications for explosive volcanism. *Earth and Planetary Science Letters*, *183*(3), 441–455. https://doi.org/10.1016/S0012-821X(00)00299-5

Mason, B. G., Pyle, D. M., & Oppenheimer, C. (2004). The size and frequency of the largest explosive eruptions on Earth. *Bulletin of Volcanology*, *66*(8), 735–748. https://doi.org/10.1007/s00445-004-0355-9

Mastin, L. G., Guffanti, M., Servranckx, R., Webley, P., Barsotti, S., Dean, K., et al. (2009). A multidisciplinary effort to assign realistic source parameters to models of volcanic ash-cloud transport and dispersion during eruptions. *Journal of Volcanology and Geothermal Research*, *186*(1), 10–21. https://doi.org/10.1016/j.jvolgeores.2009.01.008

Métrich, N, Bertagnini, A., & Di Muro, A. (2010). Conditions of Magma Storage, Degassing and Ascent at Stromboli: New Insights into the Volcano Plumbing System with Inferences on the Eruptive Dynamics. *Journal of Petrology*, *51*(3), 603–626. https://doi.org/10.1093/petrology/egp083

Métrich, Nicole, Bertagnini, A., Landi, P., Rosi, M., & Belhadj, O. (2005). Triggering mechanism at the origin of paroxysms at Stromboli (Aeolian Archipelago, Italy): The 5 April 2003 eruption. *Geophysical Research Letters*, *32*(10). https://doi.org/10.1029/2004GL022257

Métrich, Nicole, Bertagnini, A., & Pistolesi, M. (2021a). Paroxysms at Stromboli Volcano (Italy): Source, Genesis and Dynamics. *Frontiers in Earth Science*, *9*. https://doi.org/10.3389/feart.2021.593339

Métrich, Nicole, Bertagnini, A., & Pistolesi, M. (2021b). Paroxysms at Stromboli Volcano (Italy): Source, Genesis and Dynamics. *Frontiers in Earth Science*, *9*. Retrieved from https://www.frontiersin.org/articles/10.3389/feart.2021.593339

Newhall, C. G., & Self, S. (1982). The volcanic explosivity index (VEI) an estimate of explosive magnitude for historical volcanism. *Journal of Geophysical Research*, *87*(C2), 1231. https://doi.org/10.1029/JC087iC02p01231

Patrick, M. R., Harris, A. J. L., Ripepe, M., Dehn, J., Rothery, D. A., & Calvari, S. (2007). Strombolian explosive styles and source conditions: insights from thermal (FLIR) video. *Bulletin of Volcanology*, *69*(7), 769–784. https://doi.org/10.1007/s00445-006-0107-0

Pichavant, M., Di Carlo, I., Pompilio, M., & Le Gall, N. (2022). Timescales and mechanisms of paroxysm initiation at Stromboli volcano, Aeolian Islands, Italy. *Bulletin of Volcanology*, *84*(4), 36. https://doi.org/10.1007/s00445-022-01545-9

Pioli, L., Pistolesi, M., & Rosi, M. (2014). Transient explosions at open-vent volcanoes: The case of Stromboli (Italy). *Geology*, *42*(10), 863–866. https://doi.org/10.1130/G35844.1

Pistolesi, M., Delle Donne, D., Pioli, L., Rosi, M., & Ripepe, M. (2011). The 15 March 2007 explosive crisis at Stromboli volcano, Italy: Assessing physical parameters through a multidisciplinary approach. *Journal of Geophysical Research*, *116*(B12), B12206. https://doi.org/10.1029/2011JB008527

Pyle, D. M. (1998). Forecasting sizes and repose times of future extreme volcanic events. *Geology*, *26*(4), 367–370. https://doi.org/10.1130/0091-7613(1998)026<0367:FSARTO>2.3.CO;2

Pyle, D. M. (2015). Sizes of Volcanic Eruptions. In *The Encyclopedia of Volcanoes* (pp. 257–264). Elsevier. https://doi.org/10.1016/B978-0-12-385938-9.00013-4

Renzulli, A., Del Moro, S., Menna, M., Landi, P., & Piermattei, M. (2009). Transient processes in Stromboli's shallow basaltic system inferred from dolerite and magmatic breccia blocks erupted during the 5 April 2003 paroxysm. *Bulletin of Volcanology*, *71*(7), 795–813. https://doi.org/10.1007/s00445-009-0265-y

Ripepe, M., Rossi, M., & Saccorotti, G. (1993). Image processing of explosive activity at Stromboli. *Journal of Volcanology and Geothermal Research*, *54*(3), 335–351. https://doi.org/10.1016/0377-0273(93)90071-X

Ripepe, Maurizio, & Gordeev, E. (1999). Gas bubble dynamics model for shallow volcanic tremor at Stromboli. *Journal of Geophysical Research: Solid Earth*, *104*(B5), 10639–10654. https://doi.org/10.1029/98JB02734

Ripepe, Maurizio, Ciliberto, S., & Della Schiava, M. (2001). Time constraints for modeling source dynamics of volcanic explosions at Stromboli. *Journal of Geophysical Research: Solid Earth*, *106*(B5), 8713–8727. https://doi.org/10.1029/2000JB900374

Rosi, M., Bertagnini, A., Harris, A. J. L., Pioli, L., Pistolesi, M., & Ripepe, M. (2006). A case history of paroxysmal explosion at Stromboli: Timing and dynamics of the April 5, 2003 event. *Earth and Planetary Science Letters*, *243*(3), 594–606. https://doi.org/10.1016/j.epsl.2006.01.035

Rutherford, M. J., & Devine, J. D. (1996). Preeruption Pressure-Temperature Conditions and Volatiles in the 1991 Dacitic Magma of Mount Pinatubo. Retrieved October 27, 2022, from https://pubs.usgs.gov/pinatubo/ruth/

Scharff, L., Hort, M., Harris, A. J. L., Ripepe, M., Lees, J. M., & Seyfried, R. (2008). Eruption dynamics of the SW crater of Stromboli volcano, Italy — An interdisciplinary approach. *Journal of Volcanology and Geothermal Research*, *176*(4), 565–570. https://doi.org/10.1016/j.jvolgeores.2008.05.008

Schneider, H., & Barbera, F. (1998). 18 Application of order statistics to sampling plans for inspection by variables. In *Handbook of Statistics* (Vol. 17, pp. 497–511). Elsevier. https://doi.org/10.1016/S0169-7161(98)17020-7

417 Sornette, D., Knopoff, L., Kagan, Y. Y., & Vanneste, C. (1996). Rank-ordering statistics of extreme
418 events: Application to the distribution of large earthquakes. *Journal of Geophysical Research:*
419 *Solid Earth*, *101*(B6), 13883–13893. https://doi.org/10.1029/96JB00177
420 Steinberg, G. S., & Babenko, J. I. (1978). Experimental velocity and density determination of volcanic
421 gases during eruption. *Journal of Volcanology and Geothermal Research*, *3*(1–2), 89–98.
422 https://doi.org/10.1016/0377-0273(78)90005-7
423 Tournigand, P.-Y., Taddeucci, J., Gaudin, D., Peña Fernández, J. J., Del Bello, E., Scarlato, P., et al.
424 (2017). The Initial Development of Transient Volcanic Plumes as a Function of Source
425 Conditions. *Journal of Geophysical Research: Solid Earth*, *122*(12), 9784–9803.
426 https://doi.org/10.1002/2017JB014907
427 Van Eaton, A. R., Amigo, Á., Bertin, D., Mastin, L. G., Giacosa, R. E., González, J., et al. (2016).
428 Volcanic lightning and plume behavior reveal evolving hazards during the April 2015 eruption
429 of Calbuco volcano, Chile. *Geophysical Research Letters*, *43*(7), 3563–3571.
430 https://doi.org/10.1002/2016GL068076
431 Wilson, L., Sparks, R. S. J., Huang, T. C., & Watkins, N. D. (1978). The control of volcanic column
432 heights by eruption energetics and dynamics. *Journal of Geophysical Research: Solid Earth*,
433 *83*(B4), 1829–1836. https://doi.org/10.1029/JB083iB04p01829
434 Wilson, Lionel, & Self, S. (1980). Volcanic explosion clouds: Density, temperature, and particle
435 content estimates from cloud motion. *Journal of Geophysical Research: Solid Earth*, *85*(B5),
436 2567–2572. https://doi.org/10.1029/JB085iB05p02567
437 Woods, A. W., & Bower, S. M. (1995). The decompression of volcanic jets in a crater during
438 explosive volcanic eruptions. *Earth and Planetary Science Letters*, *131*(3), 189–205.
439 https://doi.org/10.1016/0012-821X(95)00012-2
440 Barberi F, Rosi M, Sodi A (1993) Volcanic hazard assessment at Stromboli based on review of
441 historical data. Acta Vulcanologica 3:173–187
442 Hort M, Seyfried R (1998) Volcanic eruption velocities measured with a micro radar. Geophys Res
443 Lett 25(1):113–116. https://doi.org/10. 1029/97GL03482

444 Hort M, Seyfried R, Vöge M (2003) Radar doppler velocimetry of volcanic eruptions: theoretical
445 considerations and quantitative documentation of changes in eruptive behaviour at stromboli
446 volcano, Italy. Geophys J Int 154(2):515–32. https://doi.org/10.1046/j.1365-
447 246X.2003.01982.x

448 Simkin T, Siebert L, McClelland L, Bridge D, Newhall C, Latter JH (1981) Volcanoes of the world: a
449 regional directory, gazetteer and chronology of volcanism during the last 10,000 years. US
450 Hutchinson Ross Publishing

451 Weill A, Brandeis G, Vergniolle S, Baudin F, Bilbille J, Fèvre JF, Piron B, Hill X (1992) Acoustic
452 sounder measurements of the vertical velocity of volcanic jets at Stromboli Volcano. Geophys
453 Res Lett 19(23):2357–2360. https://doi.org/10.1029/92GL0 2502

454

Figure caption listing

Fig. 1 Comparison between max gas velocity, as derived from ballistic ejection velocity (G_v^b), and directly measured maximum gas velocities (G_v) for major to paroxysmal eruptions at Stromboli. See Table 1 for data and sources.

Fig. 2 Relationships between MDR and maximum gas velocity (data points) and ballistic velocity (colored fields) for (a) normal, and (b) major and paroxysmal eruptions at Stromboli. Gray line gives fit obtained from Equation (4); red dashed lines represent the σ uncertainty envelope. The yellow trend is the fit to the data of Bombrun et al. (2015) and NE1 data of Harris et al. (2013), and the blue trend considers all NE crater data. Both trends look very similar, the difference with the correlation coefficient both lies in the amount of data used for each fit and because the NE2 vent data are scattered around the trendline.

Fig. 3 Rank order representation of Stromboli's normal, major and paroxysmal eruptions in terms of a) the mass discharge rate and b) the maximum gas ejection rate. Both MDR rank order and G_v rank order analyses display a gap between a higher and lower group. The dashed line marks the separation between the higher ranked group composed of paroxysmal, major and ash-dominated emissions, and the lower ranked group of ballistic-dominated normal events.

Fig. 4 MDR and G_v relations. Orange field is that defined by the data for ash-dominated emissions at Stromboli, where the positive, linear increase as a function of gas density (d_{gas}), volatile content (C_{vol}), conduit size and vent overpressure (P_{vent}), magma temperature (T) and silica content (X). The blue "Vulcanian-Plinian" field falls on a similar trend but is at a level two orders of magnitude higher than the "Strombolian" trend. Sakurajima, Mt. St. Helens and Pinatubo data fall within this field, all three being volcanoes associated with higher magma volatile content (C_{vol}), silica content (X), conduit size and vent pressure (P_{vent}) than Stromboli.

Table caption listing

Table 1 Data set for ballistic (B_v) and gas (G_v) velocities and mass discharge rate (MDR) for normal, major, and paroxysmal eruptions at Stromboli. B_v and G_v re-calculated using Equation (8) of Harris et al. (2012) are given in bold.

Table 2 Mass and duration data obtained from thermal video for normal explosions at Stromboli's NE1 and NE2 vents (derived MDR in bold).

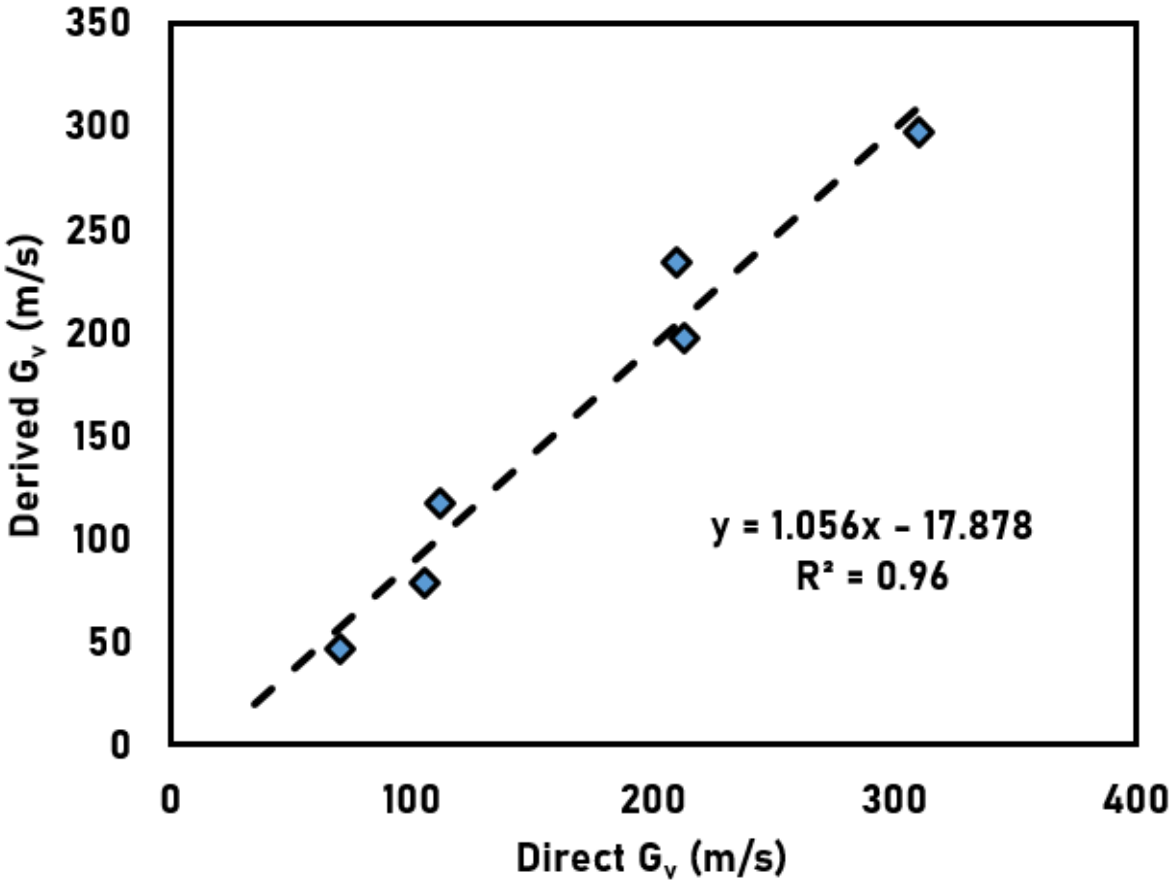

485

486 **Fig. 1**

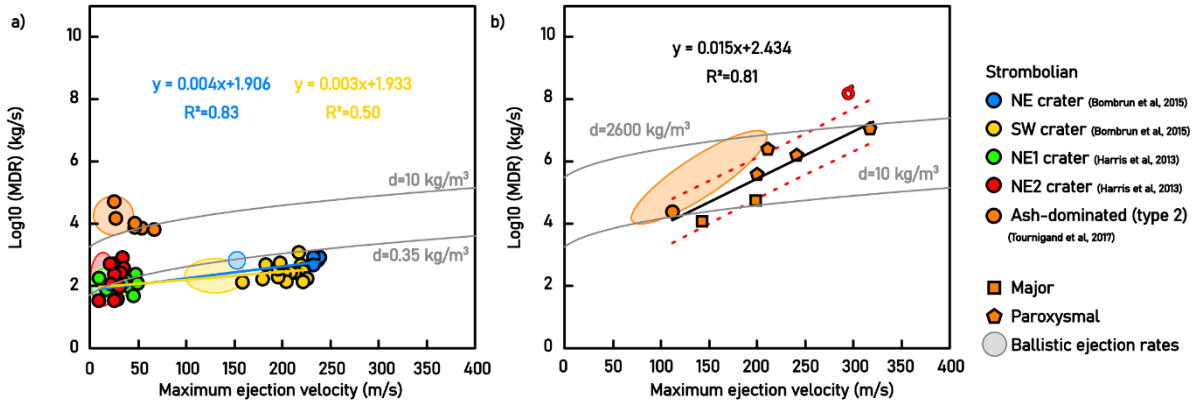

487

488 **Fig. 2**

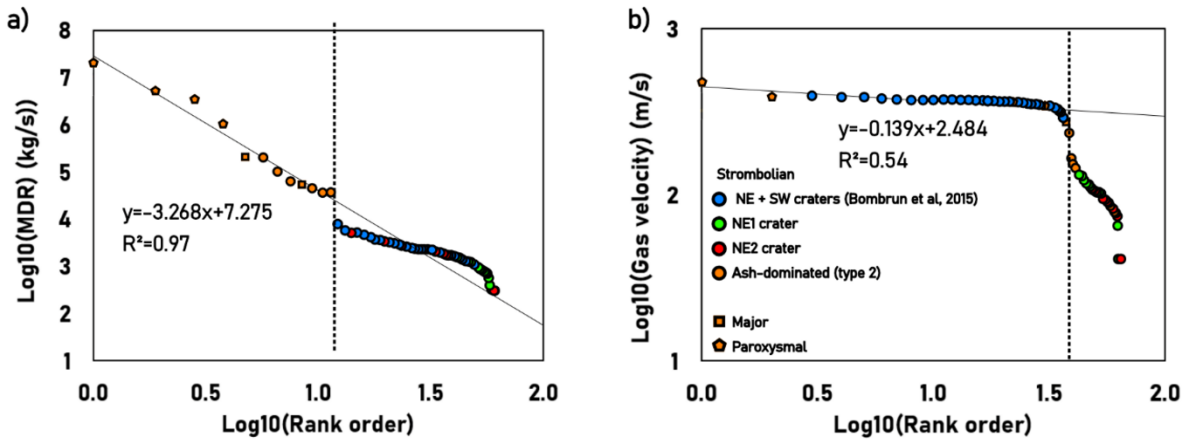
a)
Log10(MDR) (kg/s)
y=-3.268x+7.275
R²=0.97
Log10(Rank order)
b)
Log10(Gas velocity) (m/s)
y=-0.139x+2.484
R²=0.54
Strombolian
NE + SW craters (Bombrun et al, 2015)
NE1 crater
NE2 crater
Ash-dominated (type 2)
Major
Paroxysmal
Log10(Rank order)

Fig. 3

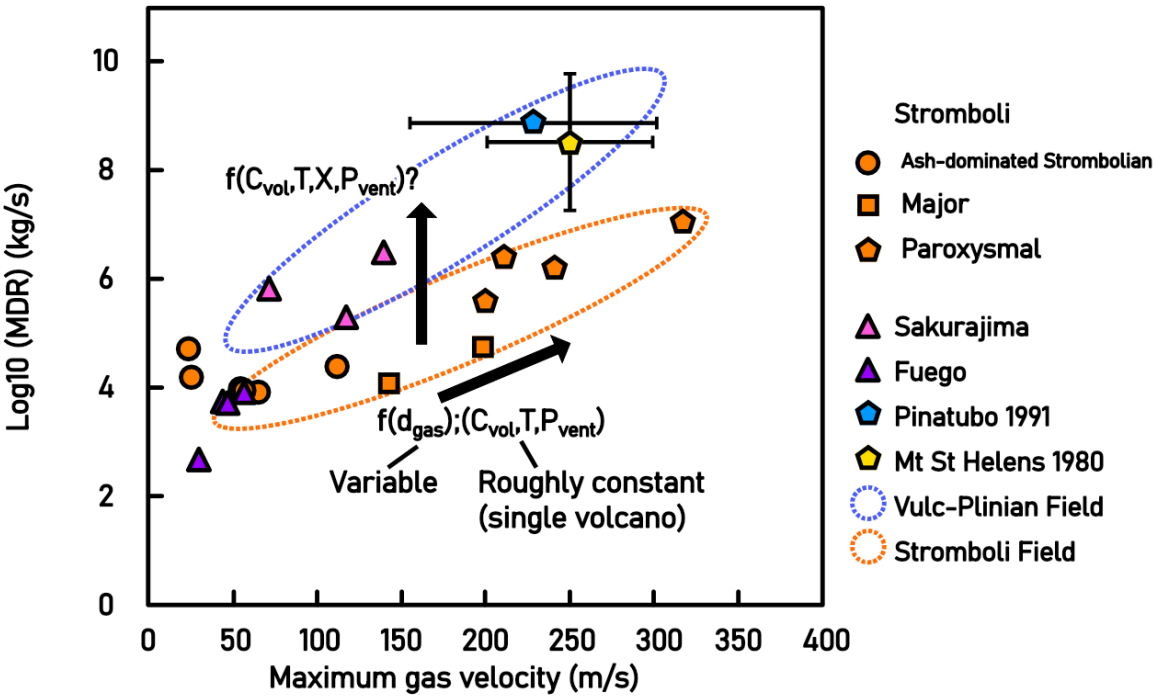
Log10 (MDR) (kg/s)
f(Cvol,T,X,Pvent)?
f(dgas);(Cvol,T,Pvent)
Variable
Roughly constant
(single volcano)
Maximum gas velocity (m/s)
Stromboli
Ash-dominated Strombolian
Major
Paroxysmal
Sakurajima
Fuego
Pinatubo 1991
Mt St Helens 1980
Vulc-Plinian Field
Stromboli Field

Fig. 4

493 **Table 1**

Date of eruption	Eruption type	Data type	Method	B_v (m/s)	Direct G_v independent measurement (m/s)	Literature derived Gv calculated (m/s)	Max derived G_v^b re-calculated (m/s)	Max derived Bv re-calculated (m/s)	Max Mass discharge rate (kg/s)	Ref.
4/5/2003	**Parox**	Radiometer Seismic	Waveform delay time	200	310		**297**		1.10E+07	Rosi et al. (2006)
4/5/2003	**Parox**	Radiometer - Seismic	Waveform delay time	185		324	**276**			Ripepe and Harris (2008)
3/15/2007	**Parox**	thermal video	Particle tracking	155	210		**234**		2.20E+06	Andronico et al. (2013), Pistolesi et al. (2011)
11/8/2009	**Major**	Bomb mapping	ballistic model	130	n.d		**199**		1.20E+04	Gurioli et al. (2013a), Pioli et al. (2014)
11/24/2009	**Major**	Bomb mapping	ballistic model	90	n.d		**142**		5.50E+04	Gurioli et al. (2013a), Pioli et al. (2014)
7/3/2019	**Parox**	Bomb mapping	ballistic model	160	n.d	200	**241**		1.40E+06	Giordano and De Astis (2020)
8/28/2019	**Parox**	Bomb mapping	ballistic model	130	n.d	200	**199**		3.60E+05	Giordano and De Astis (2020)
6/27/2004	Normal	thermal video	Gas cloud and particle tracking	129	213		**197**			Harris et al. (2012)
6/2/2010	Normal	thermal video	Gas cloud and particle tracking		8-48			**23**		Harris et al. (2013a,b)
6/8/2010	Normal	thermal video	Gas cloud and particle tracking		8-35			**14**		Harris et al. (2013a,b)
6/2004	Normal	thermal video	Particle tracking	3-101			**158**			Patrick et al. (2007)
9/27/1991	Normal	acoustic sounder	Waveform analysis	20-80			**128**			Weill et al. (1992)
9/1971	Normal	high speed camera	Particle tracking	2-72	94-112		**117**			Chouet et al. (1974)
4/2000	Normal	doppler radar	Waveform analysis	44-70			**114**			Hort et al. (2003)
9/1994	Normal	thermal video	Particle tracking	35-45	40-105		**79**			Ripepe et al. (2001)
1/29/1988 to 9/8/1989	Normal	thermal video	Particle tracking	16-22	70		**46**			Ripepe et al. (1993)
10/1/1996	Normal	doppler radar	Waveform analysis	7-13			**34**			Hort and Seyfried (1998)
27/9/2012 to 18/5/2014	Normal	thermal video	Gas cloud and particle tracking			240			1.30E+03	Bombrun et al. (2015)
26/5/2013 to 26/5/2016	Normal	Visible light and thermal video	Gas cloud and particle tracking			112			5.25E+04	Tournigand et al. (2017)

494

Table 2

Crater	Date	Time	Maximum Velocity*	Total Mass*		Duration	MDR	Log_{10}(MDR)
	(dd/mm/yy)	(hh:mm:ss)	(m s^{-1})	(x 10^3 kg)		(s)	(kg/s)	(kg/s)
NE1	2/6/2010	11:35:23	16.6	1.1	1.4	18.6	**67**	1.83
NE1	2/6/2010	11:57:51	39.5	3.5	3.8	22.9	**160**	2.20
NE1	2/6/2010	12:22:35	8.3	2.7	3	18.2	**156**	2.19
NE1	2/6/2010	14:08:51	39.5	1.7	1.8	19.0	**92**	1.96
NE1	2/6/2010	14:38:43	47.8	1.7	1.9	16.4	**110**	2.04
NE1	2/6/2010	14:59:53	37.4	3.3	3.7	28.1	**125**	2.10
NE1	2/6/2010	15:48:05	43.6	1.1	1.2	27.2	**42**	1.63
NE1	2/6/2010	16:08:17	33.3	0.9	1	9.4	**101**	2.00
NE1	2/6/2010	16:12:11	47.8	1.3	1.4	6.6	**204**	2.31
NE1	8/6/2010	13:50:46	33.3	1.3	1.4	10.2	**132**	2.12
Average			34.7	1.9	2.1	17.7	119	2.0
NE2	8/6/2010	12:43:43	22.9	2.3	2.6	5.0	**489**	2.69
NE2	8/6/2010	13:29:57	29.1	0.4	0.5	5.2	**86**	1.94
NE2	8/6/2010	14:03:17	20.8	0.32	0.35	3.4	**99**	1.99
NE2	8/6/2010	14:05:23	35.3	1.9	2.1	5.2	**385**	2.59
NE2	8/6/2010	14:20:28	27	1.1	1.2	4.8	**239**	2.38
NE2	8/6/2010	15:08:56	29.1	1.1	1.2	4.6	**250**	2.40
NE2	8/6/2010	15:19:10	33.3	1.3	1.4	5.0	**270**	2.43
NE2	8/6/2010	16:32:13	33.3	3.8	4.2	5.0	**799**	2.90
NE2	8/6/2010	17:00:32	8.3	0.09	0.1	3.0	**32**	1.50
NE2	8/6/2010	18:03:52	24.9	0.56	0.63	18.6	**32**	1.50
NE2	8/6/2010	18:20:31	27	0.13	0.15	4.2	**33**	1.52
Average			26.5	1.2	1.3	5.8	247	2.2

** data from Harris et al. (2013)*